Fault Impedance Analysis and Non-Conventional Distance Protection Settings for Half-Wavelength Transmission Line Applications

Javier Santiago Ortega, Maria Cristina Tavares

***Abstract*— This paper presents an analysis of fault phase impedance and its dynamic response for half-wavelength (HWL) transmission lines. One important issue of this technology is fault protection as distance protection elements are based on impedance for conventional AC lines. HWL line has very long length, preventing the direct application of classical impedance method because the capacitance effect produces different impedance behavior. This paper analyzes and characterizes the phase impedance response, and proposes alternative distance protection settings focusing on solving the problem of line-to-line fault detection. It is proven that the algorithm covers 84% of the line length. However, faults in the central region have a high resistance characteristic and cannot be detected with the proposed method. The paper takes into account the influence of line transpositions that further affects the protection performance near central region. Transient analysis and software in the loop tests were performed with PSCAD/EMTDC.**

***Index Terms*— Fault analysis, Distance protection, Bulk power transmission, Half-wavelength line, Impedance calculation.**

I. Introduction

Half-wavelength transmission line is a non-conventional alternative for bulk power transmission over very long distances that is attracting more attention in recent years. Large continental countries such as Brazil, Russia, and China need transmission lines with distances between 1500-3000 km to use new energy resources (hydroelectric, wind and solar plants) located far away from main load centers [1], [2],[3].

A. Motivation of research

Nowadays, transmission lines with high voltage direct current (HVDC) technology are used for very long distance transmission due to the evolution of power electronics. A transmission line with half-wavelength (HWL) properties is an alternating current (AC) non-conventional alternative that allows point-to-point transmission with outstanding steady-state properties [2], [4].

A HWL transmission line has around 2500 km for 60-Hz systems and 3000 km for 50-Hz systems, and tuning procedure allows flexible line distances [5], [6]. HWL lines may have lower costs compared to equivalent ultra-high voltage AC (UHVAC) conventional transmission systems mainly because there is no need of series nor shunt compensation, and no intermediate substations [2]. In addition, when properly designed, the HWL line cost can be 25% lower than the one of an equivalent HVDC line, mainly because power electronic converters and filters are not used [2], [7].

Despite their excellent steady-state properties, HWL lines have not been constructed, and some operative issues still require further studies. One of those topics is line protection.

B. Literature review

Looking at HWL protection and control field, some alternatives for fault location based on distance element [8], [9], fault detection based on conventional relays [10], [11], faulty phase selection [12], single-phase auto-reclosing schemes [13] and traveling wave algorithms have been proposed with promising results [14], [15]. In addition, HWL critical overvoltages due to resonant fault can be controlled using spark gaps (SGs) adequately located and coordinated [16].

Regular line protection is based on the distance principle that measures the impedance from voltage and current phasors at line terminals. Typically, there are two impedances to calculate:

a. Phase impedances (L-L) are obtained from the division of line voltage phasor variation and line current phasor variation.
b. Phase to ground (L-G) impedance are obtained dividing the phase to ground voltage phasor and the respective line current phasor adequately compensated.

Regarding fault detection using distance protection, literature shows that this method is not effective in HWL line applications. Distance elements need the assistance of other existing protection principles (overcurrent, overvoltage, undervoltage, directional and sequence quantities) to detect three-phase and line-to-Ground faults along the line [10], [11].

The distance protection problem for very long AC lines was pointed out many decades ago. The concept of complex impedance with constant angle and magnitude proportional to line length is no longer valid for lines longer than 1/8 of the wavelength [17]. Therefore, typical protection principles do not apply to HWL lines in a straightforward manner due different impedance behavior during fault occurrence.

In addition, classical phase to ground impedance compensation does not consider shunt capacitance. Some applications consider the correction of distance algorithm due to capacitance effect for lines up to 645 km – 1000 kV – 50 Hz (with intermediate substation), obtaining acceptable protection

This work was supported by the São Paulo Research Foundation (FAPESP, Projects: 2015/13823-0, 2017/20010-1), CNPq (307237/2020-6), and CAPES (code 001), Brazil.

J.A. Santiago and M.C. Tavares are with the School of Electrical and Computer Engineering, University of Campinas (UNICAMP), Av. Albert Einstein, 400, 13083-250, Campinas, SP, Brazil (e-mail: javiersa@dsce.fee.unicamp.br, ctavares@unicamp.br).

performance. However this line does present the same characteristic of the HWL line [18]. When capacitive effect with classical distance relay adjustment, but without in-deep analysis of fault impedance, is applied for HWL applications, distance protection fails for sections of the HWL line [19].

Typically, single-line to ground (SLG) fault detection in very long lines application uses zero or negative sequence quantities and directionality instead of distance protection [20]. Therefore, this paper will focus on the analysis of phase impedance and propose an alternative to detect line-to-line (LL) faults.

Phase impedance estimation in HWL lines under fault has different behavior from conventional lines because of the inductive and capacitive responses of such a long line. As a consequence, the phase fault impedance measurement equipment installed at each line terminal will observe the following characteristics [21]:

i) The fault reactance has two zero-crossing, the first at quarter-wavelength (1220 km) and the second at the half-wavelength position (2440 km). The first zero-crossing has high-resistance component. The second zero crossing has very low resistance component. Therefore, there are two zero crossing points seen by each terminal of HWL line.
ii) The equivalent source at each HWL line terminal observes a resonant condition at fundamental frequency at around 2160 km from its busbar (there can be a slight deviation associated to the terminal strength). Therefore, there are two resonant points, one for each line terminal.
iii) Supposing there is a sliding fault moving from the HWL local terminal towards the remote terminal, the local terminal will see a fault impedance with inductive-capacitive behavior. Before the first zero-crossing, the impedance presents an inductive behavior, and after that the impedance becomes capacitive until the second zero-crossing when fault impedance becomes inductive again up to the remote terminal location.

Therefore, fault impedance can be zoned conveniently according to its behavior as follows: the Zone 1 (0 -1000 km) with inductive reactance; the Zone 2 (1000-1500 km) with highly non-linear impedance that involves a zero-crossing reactance and high resistance response; and the Zone 3 (1500-2600 km) with almost linear capacitive and inductive reactance responses. In [21] it is shown that steady state faulted phase impedance can be measured in Zone 1 and 3 (84% of line length). However, transient analysis must be performed to assure a fast and correct performance of protective devices in these zones. Zone 2 does not allow an adequate impedance measurement because of the low fault current (high resistance response) and the unbalance caused by line transposition [21].

C. Contribution and paper organization

The main contributions of this paper are the robust analysis of the fault phase impedance (transient and static) response and the proposal of non-conventional setting for detection of L-L fault for HWL application using distance protection that is not possible using conventional protection criteria.

The rest of the paper is constituted as follows: the test system is described in Section II, Sections III and IV show the in-deep analysis of phase fault impedance and its transient behavior, respectively. The performance of non-conventional adjustment and logic trip for the HWL line application is shown in Section V. The main conclusions are summarized in Section VI. For transient simulations PSCAD/EMTDC software is used.

II. TEST SYSTEM

The test system is composed of a HWL transmission line at 800 kV-60 Hz slightly longer than the HWL, i.e., 2600 km. This line connects a generation station to a power grid (source-grid case). The sending station is a hydro electrical one, with 9.6 kA three-phase short-circuit current at the 800-kV busbar. The parameters of the sending system are based on a real generation station in Serra da Mesa city, Brazil. The receiving system is based on a strong Brazilian 500 kV electrical power system: 40 kA (short-circuit value).

The HWL line has eight conductors per phase (Bunting) and two ground wire (EHS 3/8"). The bundle geometry of the HWL line was designed for this study to increase the surge impedance loading (SIL) [22], respecting constraints such as the maximum electric field on the conductor surface to avoid corona effect (at 1.1 pu) and the maximum electric field on the soil. The ellipsoidal bundle geometry used is shown in Fig. 1. The adopted soil resistivity is 2000 Ω.m, typical in Brazil [23]. Table I shows the HWL electrical parameters for 60 Hz. Table II shows the system parameters. In addition, a step-down transformer station (T2) of 800/500 kV is used to connect the HWL transmission line to the power system at the receiving end. In Brazil, the 500 kV network is the largest network, and a HWL line would be connected to a step-down transformer. More detailed information of the test system is shown in [16].

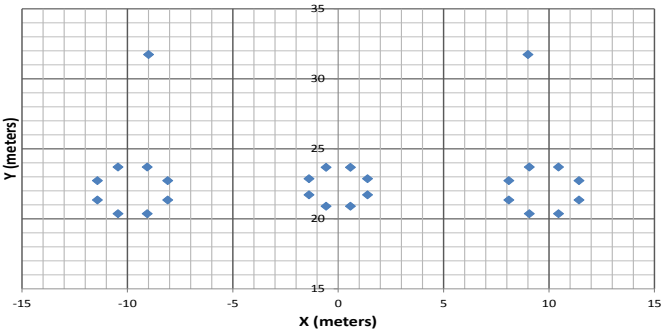

Fig. 1. Non-conventional bundle geometry. Conductors with average height.

TABLE I. Transmission (balanced) line parameters at 60 Hz

Electrical parameters		
Zero sequence		
R0 (Ω /km)	X0 (Ω/km)	B0 (μS/km)
0.3871	1.3502	4.066
Positive/negative sequences		
R1 (Ω /km)	X1 (Ω /km)	B1 (μS/km)
0.0068	0.1737	9.5367

TABLE II. Parameters of equivalent system

Source equivalent impedances	
Source	Zero Sequence (Ω)
Generation – 15 kV	0.000342 + j 0.011775
Grid System – 500 kV	7.2169 + j 36.084
Source	Positive/Negative Sequences (Ω)
Generation – 15 kV	0.000342 + j 0.011775
Grid System – 500 kV	0.4801 + j 7.201

III. Phase Impedance Characteristic for Faults In HWL Transmission Lines

In this section the steady-state fault impedance seen by relays are estimated in time-domain simulations using Fast Fourier Transform (FFT) for different fault locations. All calculations were simulated with PSCAD/EMTDC software and the results are compared with ideal phase impedance results obtained with two-port network theory.

A. *Model and simulation consideration*

The transmission line model used is the frequency dependent model in phase domain (Universal Line Model) with real transposition (TRDF).

The transposition of a 2600 km HWL line in PSCAD/EMTDC is obtained with 9 transposition cycles of 288 km each, with the sequence 1/6-1/3-1/3-1/6. This means that HWL line was split in 36 subsections and those locations were used to perform the transpositions and apply 37 discrete faults along the line. The fault points are those shown in Table III. For the two-port network cases (named as ideal) the faults were applied in rounded locations (km 1000 instead of 1011).

TABLE III. Available points of fault in km measured from sending end

Zone 1 Points (km)			Zone 2 Points (km)		Zone 3 Points (km)		
0	337	722	1107	1444	1588	1974	2310
48	433	818	1155	1492	1685	2022	2359
144	530	866	1203		1733	2070	2455
241	578	915	1300		1781	2166	2551
289	626	1011	1396		1877	2262	2600

The voltage and current phasors in PSCAD/EMTDC are calculated using FFT filter and a low pass filter (anti-aliasing). The fundamental phasors are calculated with a sampled data window considering 16 samples per cycle, which are used for phase impedance calculations.

B. *Steady-state phase impedance calculations and results*

The steady-state phase impedance seen by the relay is calculated for LL bolted faults. Figs. 2.a and 2.b show the R-X fault impedance diagram seen by sending end calculated for an ideal representation (using 60 Hz system model and two-port network elements) and phasor estimation with TRDF model in PSCAD. For PSCAD simulations, the steady-state impedance data were collected after the transient period (the transient impedance response will be analyzed in Section IV). In Fig. 2.a we see the circular locus for faults along the entire line. Faults for the first hundred kilometers have linear inductive behavior. After 400 km, the impedance locus begins to depict a circular behavior, but still with an inductive response. After 1220 km, the impedance becomes capacitive, completing the circle in the final hundreds kilometers. Fig. 2.b zooms the first 1000 km (Zone 1). It can be observed from Fig. 2.b that the impedances calculated for faults in the region 0-1000 km are similar to ideal values. Real transpositions introduce deviations as faults are applied far away from the measuring terminal. In Zone 1 the maximum deviation of the impedance calculation is 5.9% and in Zone 3 this value goes up to 13.3%.

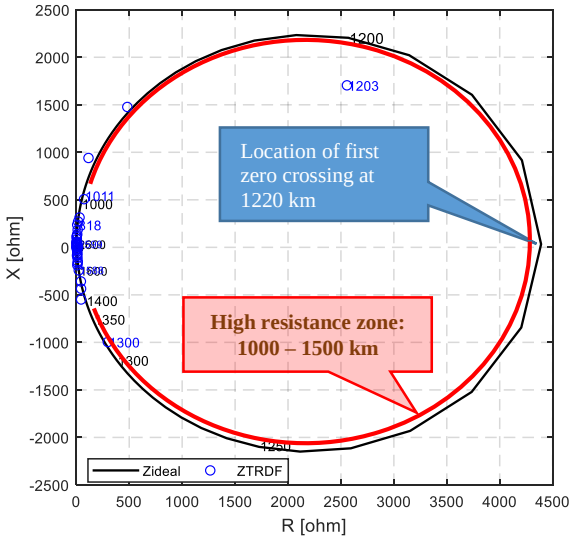

a. R-X for fault along the entire line

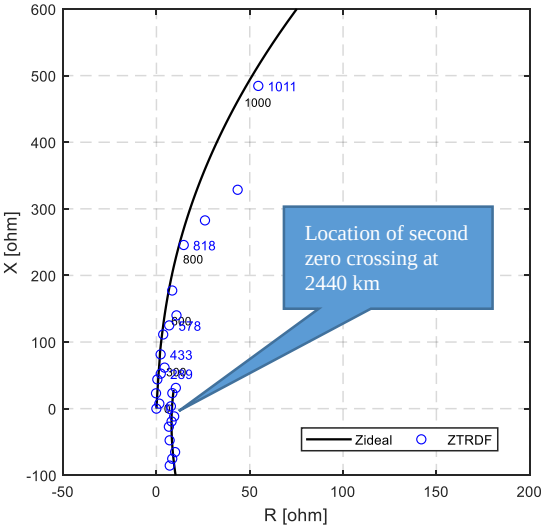

b. R-X for fault in Zone 1 (0-1000 km)

Fig. 2. R-X impedance diagram for fault along the HWL line.

C. *Influence of fault resistance, infeed effect and resonance on phase impedance estimation*

A 5-Ω fault resistance was adopted for line-to-line faults [24]. Fig. 3 shows the impedance for faults along the entire line seen by the sending end for Rf = 0 Ω and Rf = 5 Ω (calculated with two-port network technique). The impedance for the remote terminal is not presented as it looks very similar. The circle described by locus impedance diminishes for Rf = 5 Ω in the central region, while it does not deviate from the bolted fault for the rest of the line. We can say that the phase impedance estimation in Zones 1 and 3 are closer to ideal values. In central region, between 1000 km to 1500 km (Zone 2), higher deviations are observed.

Fig. 4 and Fig. 5 show the phase impedance for fault in the first 1000 km line seen by the sending end and the receiving end, respectively. In this case we show both figures because there are some different details in each case.

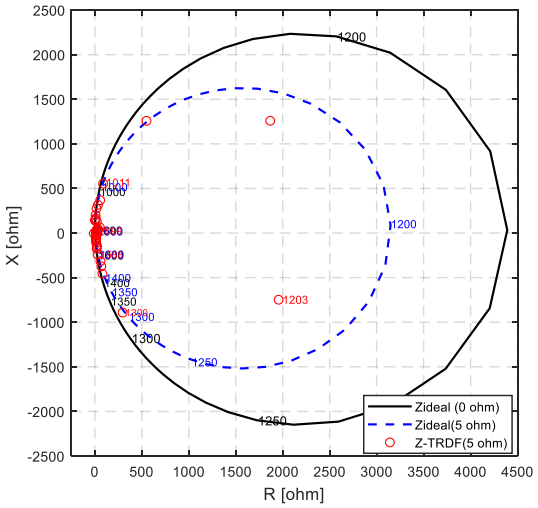

Fig 3. Rf=5 Ω, Phase AB seen by the sending end

The impedance seen by sending end with Rf = 5 Ω presents a deviation for the first 500 km, with an amplification of the resistance component. A similar phenomenon called infeed effect occurs in conventional length lines. It produces a deviation from ideal values (bolted fault) due to non-zero fault resistance when there is a remote source feeding the fault, resulting in an additional fault voltage drop. For HWL lines, it is observed a maximum deviation of 40 Ω (in R axis) for faults around 350 km that is larger than what is usually observed in conventional shorter lines. This occurs because there is a strong link between this region and the remote terminal, provoked by the fault resonance at 2250 km from the remote end (or 350 km from the sending end). Faults near the resonant region will produce a strong increase in the fault current fed by the receiving end source through the fault resistance, and this produces a high distortion of the impedance measured at the sending end. A summarized description of resonant points is shown in section I.C [25]. From 500 to 1000 km the infeed effect is reduced due to low remote fault current injection and the remaining deviations are caused by the line transpositions.

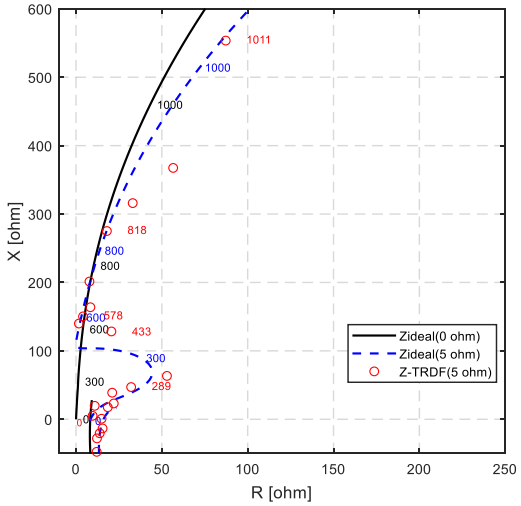

Fig 4. Zone 1 (0-1000 km), Phase AB, seen by the sending end

In a similar way, the phase impedance seen by the receiving end, shown in Fig. 5, experiences an infeed effect for faults around 440 km (measured from the receiving end). This is associated with the resonant fault for the sending source at 2160 km that provokes an increase in the remote fault current, distorting the impedance seen by the receiving end source. In this case, the deviation in the impedance measurement is around 50 Ω (in R axis), with opposite sign because both sources (sending and receiving) have a voltage phase angle larger than 180°. It is important to highlight that LL faults at resonant points have lower fault resistances producing high fault current and important infeed effect.

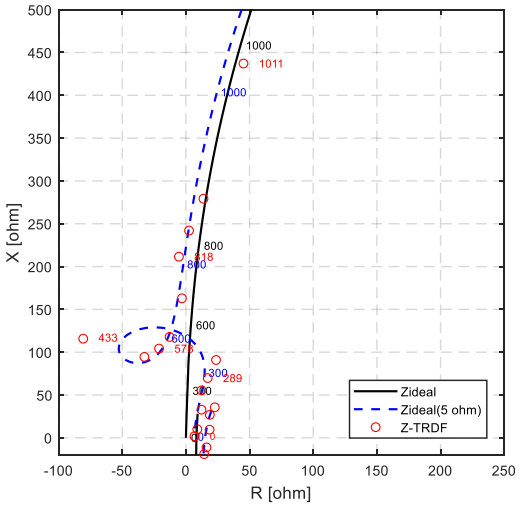

Fig 5. Zone 1 (0-1000 km), Phase AB seen by the receiving end

Fig. 6 shows the impedance seen by the sending end for faults in Zone 3 (1500-2600 km). In this region there is no infeed effect because there is no resonance associated to any terminal source. Similar response will be observed for remote terminal.

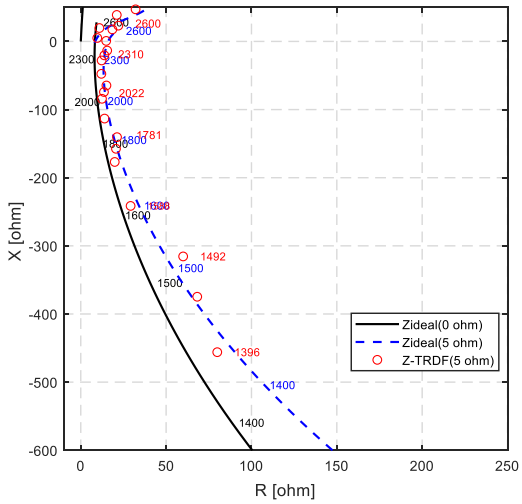

Fig 6. Zone 3 (1500-2600 km), Phase AB seen by the sending end

IV. Transient Phase Impedance Response

In Section III, the steady state phase impedance response for faults in HWL lines was characterized. The impedance traces a particular locus for LL faults along the line. Considering a digital phasor estimation process and the actual line transpositions, the steady state impedance can be adequately measured for faults in Zone 1 (0-1000 km) and Zone 3 (1500-2600 km), even though some deviations from ideal values appear. In this section, a transient phase impedance analysis is performed in order to observe its trajectory during LL faults and the time response to reach steady-state phasor response. As

mentioned in Section III, faults are applied in available points along the line in PSCAD/EMTDC as detailed in Table III.

A. Transient behavior of voltage and current phasors

This section shows the results of voltage and current (magnitude values and waveforms) seen by the sending terminal for faults at different points along the line. Fig. 7.a and Fig. 7.b are for faults at 289 km (Zone 1), 1011 km (limit of Zone 1 and 2), 1781 km (Zone 3) and 2262 km (Zone 3). Fig. 7.c shows a detail for faults at 289 km and 1011 km where the current phasors quantities reach steady state values in less than 25 ms. For faults at 1781 km the phasor presents an oscillations with pronounced magnitude excursion, taking up to 300 ms to reach steady state. For faults at 2262 km (Fig. 7.a) the current presents remarkable growth with smaller oscillation amplitude, taking up to 300 ms to reach steady state.

Fig. 7.d and Fig. 7.e show the voltage and current waveforms for faults at 1107 km, 1203 km, 1492 km (high resistance region).

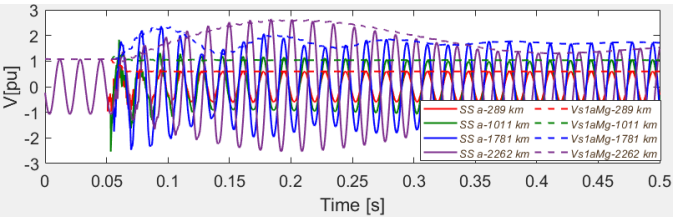

a. Voltage waveform, faults in Zones 1 and 3 – Relay at sending terminal

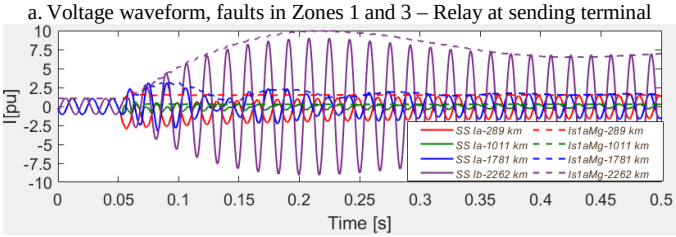

b. Current waveform, faults in Zones 1 and 3 – Relay at sending terminal

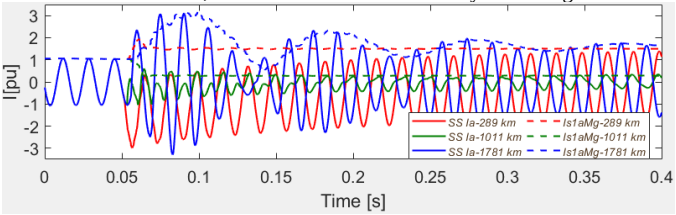

c. Detail of current waveform, faults at 289, 1011 and 1781 km

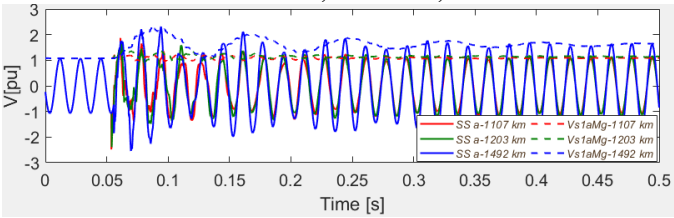

d. Voltage waveform, fault in Zone 2 – Relay at sending terminal

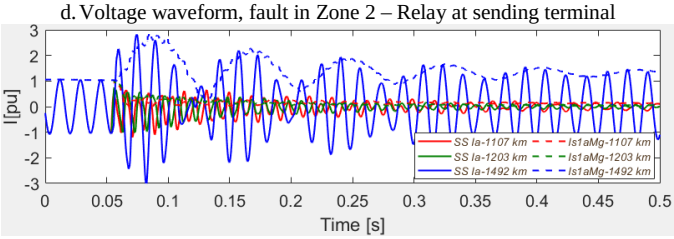

e. Current waveform, fault in Zone 2 – Relay at sending terminal

Fig.7 Voltage and current waveforms for HWL line under fault

For faults at 1107 km and 1203 km the phasors reach the steady state in around 25 ms. However, for fault at 1492 km the voltage and current phasors experience oscillations with pronounced magnitude excursion, taking approximately 300 ms to reach steady state response.

The voltage and current behavior seen by each terminal are strongly influenced by the fault impedance characteristics at fundamental frequency and the in-feed phenomenon caused by the fault resonant locations. Faults in Zone 1 have an inductive behavior that can be properly filtered by FFT filtering with regular phasor estimation process. Faults in the HWL line central region have a high resistance response. Faults between 1220-2160 km (between the first and second zero crossing reactance) have a capacitive behavior and the signals reproduce the natural response of an L-C circuit with under damped oscillations. These oscillations damp slowly and are not efficiently filtered by regular FFT filtering in the phasor estimation process. In addition, faults closer to the resonant point seen by each remote terminal (2160 km) produce a disturbance with remarkable voltage and current excursions at fundamental frequency.

For better understanding of HWL line under phase faults and what kind of components are involved in waveforms, an additional analysis is made using the Fast Fourier Transform (FFT) algorithm to calculate the Discreet Fourier Transform (DFT). For this task, the MATLAB FFT function was used.

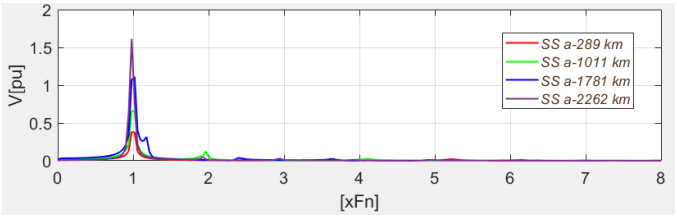

a. FFT analysis of voltage for faults at 289 km, 1011 km, 1781 km, 2262 km

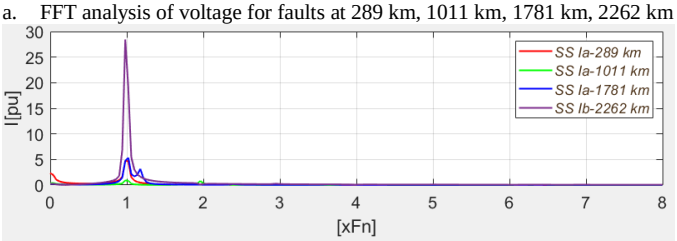

b. FFT analysis of current for faults at 289 km, 1011 km, 1781 km, 2262 km

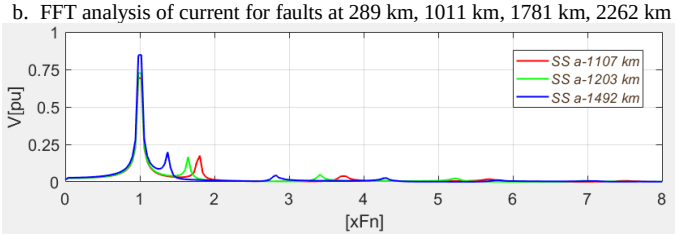

c. FFT analysis of voltage for faults at 1107 km, 1203 km and 1492 km

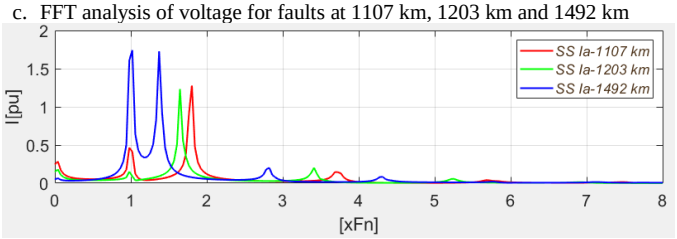

d. FFT analysis of current for faults at 1107 km, 1203 km and 1492 km

Fig.8 FFT analysis of waveforms in HWL line under fault

The time window evaluated ranges from fault inception (50 ms) up to 400 ms, in order to establish an average behavior during signal oscillations. Fig. 8 shows the Fourier analysis of voltage and current signals for faults at the same points evaluated above.

Fig. 8.a and Fig. 8.b show voltage and current FFT analysis for faults at 289 km (Zone 1), 1011 km (limit of Zone 1 and 2), 1781 km (Zone 3) and 2262 km (Zone 3). It is observed that for faults closer to the sending terminal, the fundamental component is smaller and harmonics components are lower. As the fault approaches the resonant point (2160 km), the fundamental component enlarges, and lower harmonic and inter-harmonic components will appear (between 1st and 2nd harmonics) for faults before resonant point (as for 1781 km) or subharmonic component for fault after the resonant point (as for 2262 km).

Fig. 8.c and Fig. 8.d show FFT voltage and current analysis for faults at 1107 km, 1203 km, 1492 km (region where phase impedances present high resistance response). Moderate inter-harmonic voltage components and important inter-harmonic current components appear, for the range between 1st and 2nd harmonics.

As seen, an adequate phasor quantity measurement can be made in Zone 1. For Zone 3, the phasor quantities can be affected by inter-harmonic components, but in a moderate level. We can state that a proper phasor quantity measurement for faults in Zone 2 is not possible with typical digital filters, especially for current signals, because of inter-harmonic components. These results are valid for both terminals.

B. Transient response of resistance and reactance values

Fig. 9.a shows the R-X values for faults at 289 km (Zone 1), 578 km (Zone 1), 866 km (Zone 1) and 1011 km (limit of Zone 1 and 2). In the first hundreds of kilometers (289 km and 578 km) both resistance and reactance responses are flat (stable) in less than 25 ms, as observed in conventional shorter AC lines. However, for faults applied at 866 and 1011 km, the resistance and reactance responses further oscillate, and that behavior goes up to 100 ms. The damping is reduced as the fault is applied farther from the line terminal, and R response presents higher oscillations.

Fig. 9.b shows the R-X values for faults at 1781 km, 2160 km and 2600 km (Zone 3). Larger oscillations are observed for faults at 1781 km (the capacitive region), and almost 150 ms are necessary to properly stabilize the signal. The phase impedance measurement for faults applied at 2160 km (resonant point) goes promptly to steady state values (after 30 ms). Faults farther from resonant point (2600 km) have lower oscillation amplitude, but still take around 100 ms to present a steady response.

Fig. 9.c shows the R-X values for faults at 1107 km, 1203 km and 1492 km (Zone 2). Here higher oscillations that do not attenuate are observed. For fault at 1203 km the highest oscillation amplitude for R is observed, reaching 1500 Ω. Even after 500 ms the signal still experiences oscillations. As the fault is applied farther from the line center (1492 km), the R-X oscillations are reduced. Behavior of R-X components are coherent with the analysis presented in Section IV.A.

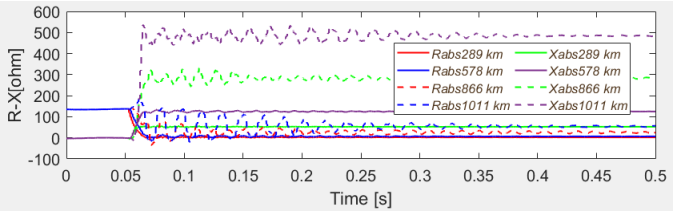

a. Phase impedance in Zone 1

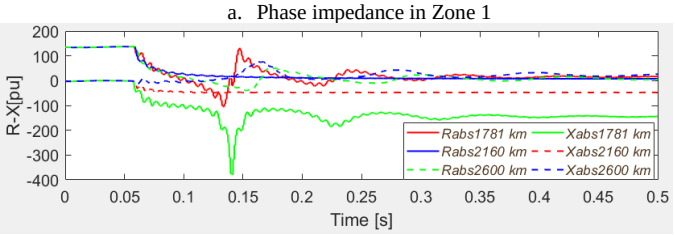

b. Phase impedance in Zone 3

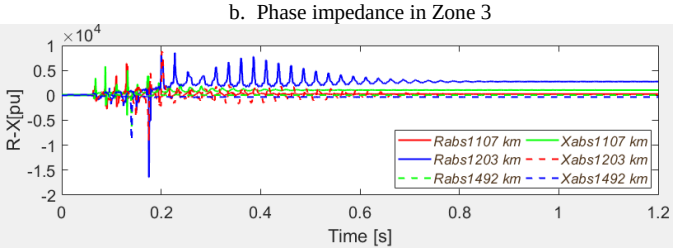

c. Phase impedance in Zone 2

Fig.9 Phase impedance transient behaviour – Sending end relay

V. Protection Configuration

A. Protection zones and faulty phase detection scheme

Based on previous analysis, protection functions were defined for Zone 1 and Zone 3, where impedance can be measured.

For Zone 1 it is proposed mho element and quadrilateral element as shown in R-X locus diagram presented in Fig. 10.a The setting of the mho element is defined to trip for faults up to 600 km. The setting is based on total fault impedance, including series inductive part and shunt capacitive part. This mho element must also cover the impedance measurement deviation provoked by fault resistance and infeed effect. An additional quadrilateral element is set to trip for faults up to 1000 km. The quadrilateral element is defined by a four-point polygonal element that covers the impedance of the first 1000 km.

For Zone 3 the quadrilateral element is defined as presented in Fig. 10.a. The quadrilateral element is positioned at fourth R-X plane quadrant and is not a reverse element. The quadrilateral element is defined by a four-point polygonal element that covers the impedance of last 1100 km. The mho element is not needed as there is no infeed effect. This quadrilateral element protects the entire Zone 3 region. The setting is defined considering total fault impedance response, coping with series inductive and shunt capacitive effects.

The adjustments of the protection zones are shown in Table IV.

A tripping logic was implemented to generate a trip signal when the any phase impedance enters the mho or quadrilateral elements regions defined in the settings defined in Table IV, that means a typical OR logic. The logic is depicted in Fig. 11, where it is shown one mho element and two quadrilateral elements (Zone 1 and Zone 3) for each terminal end of line. In addition, a typical transfer trip scheme was applied considering 12 ms (3/4 cycle) delay between the terminals.

TABLE IV. Setting of Protection Elements – R-X in ohms-prim.

	Sending Relay			Receiving Relay	
Mho	Z=130.1 Ω	Θ=88.2º	Mho	Z=150.1 Ω	Θ=91.6º
Quadril. Zone 1	R1= -32 Ω	X1=8 Ω	Quadril. Zone 1	R1= -32 Ω	X1=8 Ω
	R2= 16 Ω	X2= -4 Ω		R2= 16 Ω	X2= -4 Ω
	R3=157.5 Ω	X3= 720 Ω		R3=157.5 Ω	X3= 720 Ω
	R4= -32 Ω	X4= 720 Ω		R4= -32 Ω	X4= 720 Ω
Quadril. Zone 3	R1=-2 Ω	X1=20 Ω	Quadril. Zone 3	R1=-2 Ω	X1=20 Ω
	R2= -2 Ω	X2= -728 Ω		R2= 2 Ω	X2= -728 Ω
	R3= 225 Ω	X3= -728 Ω		R3= 2255 Ω	X3= -728 Ω
	R4= 27 Ω	X4= 25 Ω		R4= 27 Ω	X4= 25 Ω

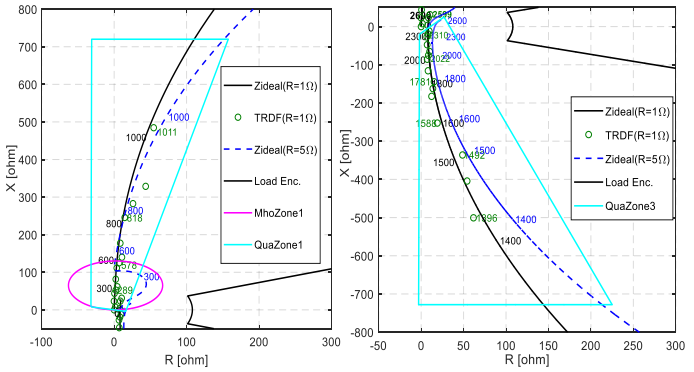

(a) Mho and quadrilateral zone protection

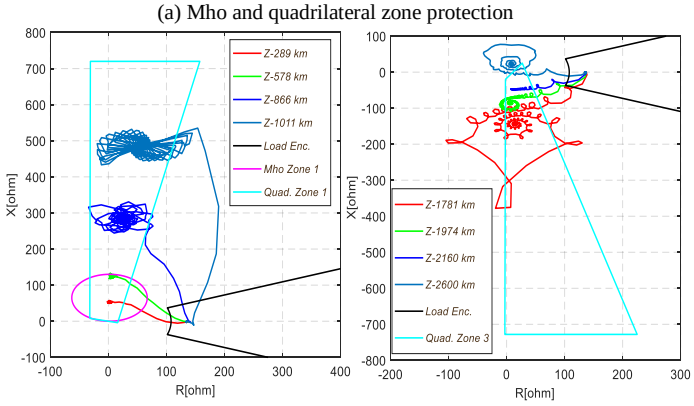

(b) R-X locus diagram of phase impedance during fault

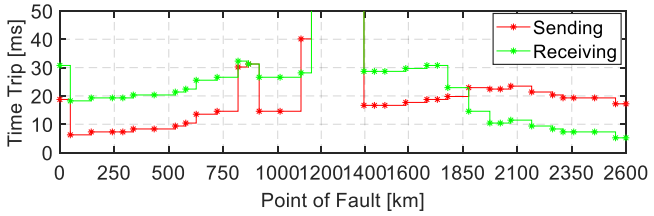

(c) Sending and receiving relay time with transfer trip

Fig. 10. LL fault detection in HWL line using phase impedance measurement.

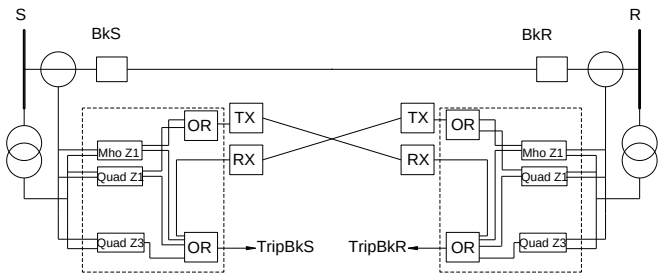

Fig. 11. Trip logic using Mho and Quadrilateral elements

B. *Performance of element zones*

Fig. 10.b shows the R-X dynamic locus. For Zone 1, faults were applied at 289 km, 578 km, 866 km and 1011 km (For practical purpose 1011 km was considered in Zone 1). It can be observed that the impedance moves towards the tripping area. For the first hundred kilometers, the phase impedance has a stable response. For the border zone, 866 km and 1011 km, the phase impedance experiences the oscillations analyzed in last section before becoming stable. However, the impedance remains inside the defined tripping region. As faults are applied farther from its terminal (above 700 km, approximately), the impedance oscillates and takes more time to reach the trip region.

For Zone 3, faults were applied at 1781 km, 1974 km, 2160 km and 2600 km. It is observed that the impedance moves towards the protection trip region. As fault is closer to the second zero crossing (2440 km), lower oscillations are observed. However, the phase impedance for fault at 2600 km does not enter in quadrilateral element of Zone 3, instead it goes to Zone 1.

Fig 10.c shows the final tripping time for relays at the sending and the receiving terminals considering the transfer trip scheme applied. Faults in Zone 1 and Zone 3 can be detected by both terminals with tripping times between 10 ms to 30 ms.

The Zone 3 quadrilateral element has delayed time response that can vary between 25-50 ms for faults between 1500–1800 km and 2500-2600 km, and from 50 ms to 175 ms for faults between 1800-2500 km. Therefore, faults in Zone 3 should be supported by a transfer trip from Zone 1 of the opposite terminal to speedup tripping time.

C. *Final remarks*

The presented line protection can detect faults in Zone 1 (0-1000 km) and Zone 3 (1500-2600 km), what represents 84% of the entire line length, within 8 ms to 30 ms. The response takes longer as the fault is applied farther from the relay location. However, it must be clearly stated that Zone 2 (1000-1500 km) cannot be protected with the distance function setting proposed due to the inability to measure adequately the fault phase impedance. This problem arises from the natural low fault current magnitude further compromised by the unbalance produced by line transpositions. Additionally, higher inter-harmonic components prevent the correct phasor measurement when applying digital filters available in commercial relays. Therefore, a complementary protection element must be proposed to detect faults in Zone 2.

Another important aspect is the need to implement a coordination method to discriminate faults close to both terminals (0 – 100 km and 2440 – 2600 km). The measured phase impedance in both regions falls in the first quadrant of R-X impedance plane as shown in Fig. 2.b. Finally, it is necessary to have a transfer trip with a communication channel to reduce the tripping time for faults at Zone 3 (1500 to 2600 km).

VI. Conclusions

This paper presents a detailed study of the phase impedance behavior for line-to-line faults in HWL lines. The phase impedance response is not similar to regular long lines. Even though, it is possible to apply regular distance protection

elements with adequate criteria. Two zones can be considered, specifically Zone 1, between 0-1000 km, and Zone 3, between 1500-2600 km.

To set the distance protection elements for the two defined zones, the inductive/capacitive impedance components of HWL line must be taken into account. The distance protection element functions, mho and quadrilateral, can be applied for Zone 1, resulting in total tripping time between 8-30 ms. For Zone 3 just quadrilateral is element is used, but a transfer trip scheme between both terminals is necessary to achieve adequate tripping times. The Zone 3 quadrilateral element has larger tripping times due to high resistance response and the presence of inter-harmonic components, resulting in longer time to obtain stable voltage and current phasors using regular filtering methods.

An important infeed effect is observed at Zone 1 provoked by resonant faults associated to the remote terminal source. However, this effect can be properly dealt with by mho element of the proposed protection scheme.

It is important to notice that to properly protect the entire HWL line it is still necessary to propose fault detection algorithms for Zone 2, which has a natural high resistance response. Besides, it is necessary to discriminate faults close to local terminal from the ones at remote terminal, as both fault impedances fall in the first quadrant of R-X impedance plane. In forthcoming material, the mitigation method proposed in literature to remove resonant faults (i.e. spark gaps in the middle of line) will be considered altogether with the protection system.

The HWL line protection response was tested in a software in the loop (SIL) environment.

VII. References

[1] J. Sun, M. Li, Z. Zhang, T. Xu, J. He, H. Wang, and G. Li, "Renewable energy transmission by HVDC across the continent: system challenges and opportunities," in CSEE Journal of Power and Energy Systems, vol. 3, pp. 353–364, Dec. 2017.

[2] C. Portela, J. Silva, and M. Alvim, "Non-Conventional AC Solutions Adequate For Very Long Distance Transmission – An Alternative For The Amazon Transmission System," in *Proc. IEC/CIGRE UHV Symposium*, Beijing, China, 2007.

[3] J. Jia, J. Yi, A. Wang, W. Lin, W. Zhong, and S. Cheng, "Research on the Operation Mode Construction and Stability Control Measures of Half-WaveLength Transmission Test System," *Proc. ISPEC 2019 - 2019 IEEE Sustain. Power Energy Conf. Grid Mod. Energy Revolution*, pp. 252–257, Beijing, China, 2019.

[4] F. Iliceto and E. Cinieri, "Analysis of half-wave length transmission lines with simulation of corona losses," IEEE Trans. Power Deliv., vol. 3, no. 4, pp. 2081–2091, Oct. 1988.

[5] J. S. Ortega and M. C. Tavares, "New perspectives about AC Link based on Half-Wavelength Properties for Bulk Power Transmission with Flexible Distance," IET Gener. Transm. Distrib., vol. 12, no. 12, pp. 3005–3012, May. 2018.

[6] F. S. Prabhakara, K. Parthasarathy, and H. N. R. Rao, "Performance of Tuned Half-Wave-Length Power Transmission Lines," IEEE Trans. Power Appar. Syst., vol. PAS-88, no. 12, pp. 1795–1802, Dec. 1969.

[7] G. Samorodov, S. Kandakov, S. Zilberman, T. Krasilnikova3, M. C. Tavares, C. Machado Jr., Q. Li, "Technical and economic comparison between direct current and half-wavelength transmission systems for very long distances," IET Gener. Transm. Distrib., vol. 11, no. 11, pp. 2871–2878, Jul. 2017.

[8] F. V. Lopes, B. F. Küsel, K. M. Silva, D. Fernandes, and W. L. A. Neves, "Fault location on transmission lines little longer than half-wavelength," Electr. Power Syst. Res., vol. 114, pp. 101–109, May. 2014.

[9] R. G. Fabián, "Distance Protection for Half-Wavelength Power Transmission Lines (In Portuguese)," Ph.D dissertation, Elec. Comp. Eng. School, Univ. Campinas, Brazil, 2015.

[10] E. C. Gomes, M. C. Tavares, and C. A. Floriano, "Protection Scheme for Single-Phase Fault along a Half Wavelength Transmission Trunk Using Conventional Relay," *in Proc. International Conference on Power Systems Transients* (IPST2013), 2013.

[11] R. G. Fabián and M. C. Tavares, "Using of Conventional Relays for Protecting Half-Wavelength Transmission Line from Three-Phase Faults," *in Proc. International Conference on Power Systems Transients*, 2013.

[12] R. Fabián and M. C. Tavares, "Faulted Phase Selection for Half-Wavelength Power Transmission Lines," IEEE Trans. Power Deliv., vol. 33, no. 2, pp. 992–1001, Apr. 2018.

[13] O. Dias and M. C. Tavares, "Single-Phase Auto Reclosing Mitigation Procedure for Half Wavelength," IET Gener. Transm. Distrib., vol. 11, no. 17, pp. 4324 – 4331, Oct. 2017.

[14] N. Tong, L. Chen, W. Wang, X. Lin, and Z. Li, "Local-Measurement-Based High-Speed Protection," IEEE Trans. Power Deliv., vol. 35, no. 5, pp. 2481–2494, Oct. 2020.

[15] L. Tang and X. Dong, "A travelling wave differential protection scheme for half-wavelength transmission line," Int. J. Electr. Power Energy Syst., vol. 99, no. January, pp. 376–384, Feb. 2018.

[16] J. S. Ortega and M. C. Tavares, "Transient Analysis and Mitigation of Resonant Faults on Half-Wavelength Transmission Lines," IEEE Trans. Power Deliv., vol. 8977, pp. 1–1, Aug. 2019.

[17] L. M. Wedepohl and S. E. T. Mohamed, "Apparent impedances of very long multiconductor transmission lines," Proc. Inst. Electr. Eng., vol. 117, no. 7, p. 1373, Jul. 1970.

[18] Z. Y. Xu, S. F. Huang, L. Ran, J. F. Liu, Y. L. Qin, Q. X. Yang, and J. L. He, "A distance protection relay for a 1000-kV UHV transmission line," IEEE Trans. Power Deliv., vol. 23, no. 4, pp. 1795–1804, Oct. 2008.

[19] A. G. De Castro, L. A. Soares, M. R. Araujo, W. B. F. Drumond, A. L. M. Coelho, and I. P. Faria, "Performance analysis of non-conventional distance protection and phase selection algorithms in transmission lines little longer than half-wavelength," *in Proc.* "13th IEEE International Conference on Industry Applications, INDUSCON", pp. 1008–1015, 2019.

[20] G. E. Alexander, J. Mooney, and W. Tyska, "Advanced Application Guidelines for Ground Fault Protection," in Western Protective Relay Conference, 2001, Oct. 1997.

[21] J. A. Santiago Ortega and M. C. Dias Tavares, "Fault Impedance Analysis in Half-Wavelength Transmission Lines," *in Proc.* VII Brazilian Symposium of Electrical Systems, São Paulo, Brazil, pp. 1–6, 2020.

[22] J. S. Acosta and M. C. Tavares, "Methodology for optimizing the capacity and costs of overhead transmission lines by modifying their bundle geometry," Electr. Power Syst. Res., vol. 163, no. Part B, pp. 668–677, Oct. 2017.

[23] C. Medeiros Portela, M. Cristina Tavares, J. Pissolato Filho. "Accurate representation of soil behaviour for transient studies", IET GTD, Vol. 150, Issue 6, p. 736 – 744, Nov. 2003.

[24] V. De Andrade and E. Sorrentino, "Typical expected values of the fault resistance in power systems," *in Proc.* IEEE/PES Transmission and Distribution Conference and Exposition: Latin America, T and D-LA, pp. 602–609, Sao Paulo, Brazil, 2010.

[25] J. Santiago and M. C. Tavares, "Relevant factors for temporary overvoltages due to fault-resonance conditions on half-wavelength transmission lines," Electr. Power Syst. Res., vol. 175, no. April, p. 12, 2019.